Transport analysis of air-gap membrane distillation

A.M. Alklaibi, Noam Lior *

Department of Mechanical Engineering and Applied Mechanics, University of Pennsylvania, Philadelphia, PA 19104-6315, USA

Abstract

The air gap membrane distillation process has been modeled as a two-dimensional conjugate problem in which a simultaneous numerical solution of the momentum, energy and diffusion equations of the feed and cold solutions have been carried out. The results were validated in comparison with available experimental results. The modeling and sensitivity analyses provide useful basic detailed information about the nature of the process, and are helpful for process improvement and optimization. Some of the principal conclusions are: (1) the air/vapor gap has the major role in reducing the parasitic heat loss in the process, (2) the gap width has an important effect: decreasing it five-fold increases the permeate flux 2.6-fold, but the thermal efficiency improves only slightly because the conductive heat loss increases too, (3) increasing the inlet temperature of the hot solution has a major effect on the permeate flux and also increase the thermal efficiency, while decreasing the coolant temperature has a lesser effect on the flux increase, and even slightly reduces the efficiency, (4) the feedwater salt concentration has a very small effect on the permeate flux and thermal efficiency, (5) the inlet velocities of the hot and cold solutions have a relatively small effect, (6) reducing the thermal conductivity of the membrane material improves the process thermal efficiency somewhat, and the permeate flux more strongly.
© 2005 Elsevier B.V. All rights reserved.

Keywords: Membrane distillation; Water desalination; Transport through membranes; Distillation; Air gap membrane distillation

1. Introduction

Membrane distillation (MD) for water desalination is a membrane technique for separating water vapor from a liquid saline aqueous solution by transport through the pores of hydrophobic membranes, where the driving force is the vapor pressure difference created by temperature difference across the membrane (cf. [1]). A variety of methods may be employed in MD, such as (i) direct contact membrane distillation (DCMD) in which the membrane is in direct contact with liquid phases in both sides (cf. [2–4]). (ii) Air gap membrane distillation (AGMD) in which an air layer is interposed between the membrane and the condensation surface (cf. [5,6]); (iii) vacuum membrane distillation (VMD) in which a vacuum is applied to increase or establish the vapor pressure difference between the membrane sides and the condensation takes place in an external condenser (cf. [7,8]). (iv) Sweep-

ing gas membrane distillation (SGMD) in which a stripping gas is used on the cold side to sweep the permeate away, with condensation in a separate device (cf. [9–13]).

MD has many significant advantages, such as high system compactness, possibility to operate at low temperatures (∼30–90 °C) which makes it amenable for use with low temperature heat sources, including waste or solar heat, and, when compared with say reverse osmosis or electrodialysis, the simplicity of the membrane which allows it to be manufactured from a wide choice of chemically and thermally resistant materials, and much larger pores than of reverse osmosis membranes (and typically larger than in ultra-filtration membranes, [1]) that aren't nearly as sensitive to fouling. It was not as yet adapted for commercial use in water desalination, in part because of some negative views about the economics of the process [14], which were, however, formed long ago, on a far-from-optimal membrane and model, and which seem also to contain calculation errors which overestimate the cost significantly. Another uncertainty is a lack of long-term operation data with natural saline waters to ascertain the sta-

---

* Corresponding author. Tel.: +1 215 898 4803; fax: +1 215 573 6334.
  E-mail address: lior@seas.upenn.edu (N. Lior).

bility of the hydrophobicity of the membranes. The advantages of MD, and continuing improvements in membranes driven by alternative markets for such products (such as the Goretex® membrane used widely in the clothing and shoe industry), make it worthwhile to explore this process in more detail. A recent state of the art review of MD and assessment of the process potential can be found in [15].

The most common approach to modeling MD, as found in the literature, is by assuming the process as one-dimensional and applying empirical heat and mass transfer coefficients. In this approach, (cf. [16–18]) a semi-empirical model is developed, in which the permeate flux is expressed in term of the bulk temperatures of the hot and the cold fluids, and the thermal and concentration effects are expressed in terms of simplified temperature and concentration "polarization" terms, determined, alongside with the heat and mass transfer coefficients, empirically.

Two past studies were performed with first attempts to introduce two-dimensional analysis to AGMD, at least partially, but they were not of general nature. One is an attempt [19] to assess by a numerical model the effects of the natural convection in the air/vapor gap on the permeate flux. A two-dimensional model of laminar natural convection was developed and solved for the gap, but not in the hot feed and coolant channels. The model is thus not conjugate, and was not validated. They found that the heat transfer across the gap is primarily conductive and one-dimensional for gap thicknesses < 5 mm anyway, and one can conclude that natural convection can be ignored since practical gap thicknesses are smaller. A two-dimensional numerical analysis, but only of the saline feedwater channel, was conducted in [20] to evaluate the supersaturation distribution of $BaSO_4$ in regard to its possible membrane scaling effects. An iterative numerical scheme (rather than a conjugate one as done in our paper), as well as several significantly simplifying assumptions, were employed, and the model was not validated.

This paper presents a transport analysis based on two-dimensional conjugate model in which, the temperature and concentration of the hot and cold solutions not only normal to the membrane (y-direction in this paper) but also along the membrane (x-direction) are part of the solution so that its sensitivity to the major design parameters could be better evaluated. In that, the permeate flux is computed locally along the hot side of membrane (i.e. function of x), and the length-averaged permeate flux is the resulting integration of the local fluxes along the membrane.

In addition to the full description of the flow, temperature and concentration fields in the hot and cold solutions, the effects of the membrane, air gap, condensate film, and cooling plate are computed and shown.

An analysis of the sensitivity of the production rate to the major operating parameters was conducted. These parameters include the inlet temperature of the hot solution, T_{hi}, in the range 40–80 °C, the inlet temperature of the cold solution, T_{ci}, in the range 5–45 °C, the concentration of the feed solution, w_{si}, in the range 20,000–50,000 ppm, the inlet ve-

locity of the hot (u_{hi}) and cold (u_{ci}) solutions in the range 0.1–0.3 m/s, the air gap width, δ_g, in the range 1–5 mm, and the thermal conductivity of the membrane, k_m, in the range 0.05–0.3 $Wm^{-1} K^{-1}$.

2. Model development

The distillation process takes place in the domains shown in Fig. 1a, that are the hot solution (h), membrane (m), air/vapor gap (g), condensate film (f), cooling plate (p), and the cold fluid (c). For further clarification, Fig. 1b shows the thermal resistances in the considered model. We model the process by solving the 2-dimensional (this is based on the practical assumption that the third dimension, the channel width, is relatively large) momentum, energy and species equations in the feed and cold solutions regions. By a coupling technique of the boundary conditions at the hot membrane surface and cooling plate cold surface, the effect of the membrane, air/vapor gap, condensate film, and cooling plate are considered. The maximum Reynolds number is 1390 and the flow is laminar. The model equations in each of the domains of Fig. 1 are developed below.

2.1. The hot solution region

The hot saline solution flows between two parallel hydrophobic microporous membranes. The flow is symmetric along the flow direction, and so only half of the cell is shown. The transport of the momentum, energy, and species of the hot
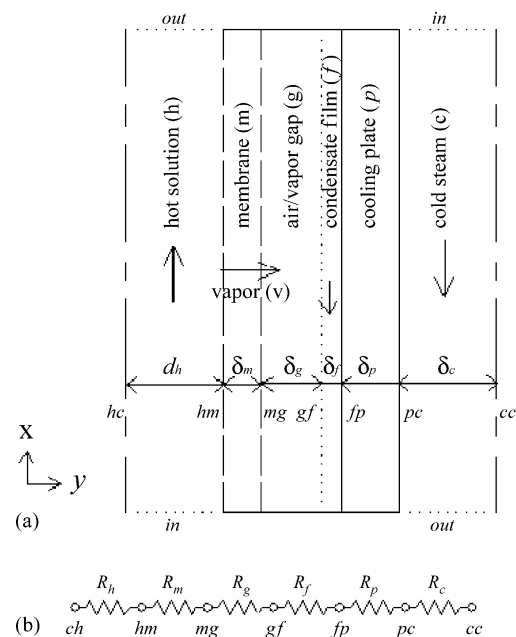

Fig. 1. (a) The AGMD model with domain and interface labels. The base-case model dimensions are $d_h = 2$ mm, $l_m = 0.2$ m, $\delta_m = (4) 10^{-4}$ m, $\delta_g = (4) 10^{-3}$ m, $d_p = (1.5) 10^{-3}$ m, $d_p = (2) 10^{-3}$ m. (b) The thermal resistances in the model.

solution are described by the continuity, momentum, energy and species conservation equations, which are normalized by using the dimensionless variables

$$\bar{x}_h = \frac{x_h}{d_h}, \quad \bar{y}_h = \frac{y_h}{d_h}$$

$$\bar{u}_h = \frac{u_h}{u_{hi}}, \quad \bar{v}_h = \frac{v_h}{u_{hi}},$$

$$\bar{P}_h = \frac{P_h}{\rho_S u_{hi}^2},$$

$$\bar{T}_h = \frac{T_h - T_{ci}}{T_{hi} - T_{ci}}, \quad \bar{w}_s = \frac{w_s}{w_{si}}$$ (1)

where d_h is the distance between the membrane surface and the center of the hot solution channel, u_{hi} and u_{ci} are the inlet velocity of the hot and cold solutions, T_{hi} and T_{ci} are the inlet temperature of the hot and cold solutions, and w_{si} is the mass fraction of salt (here NaCl) in water at the entrance of the channel.

The dimensionless equations are thus

$$\frac{\partial \bar{u}_h}{\partial \bar{x}_h} + \frac{\partial \bar{v}_h}{\partial \bar{y}_h} = 0$$ (2)

$$\bar{u}_h \frac{\partial \bar{u}_h}{\partial \bar{x}_h} + \bar{v}_h \frac{\partial \bar{u}_h}{\partial \bar{y}_h} = -\frac{\partial \bar{P}_h}{\partial \bar{x}_h} + \frac{1}{Re_h}\left(\frac{\partial^2 \bar{u}_h}{\partial \bar{x}_h^2} + \frac{\partial^2 \bar{u}_h}{\partial \bar{y}_h^2}\right)$$ (3)

$$\bar{u}\frac{\partial \bar{v}_h}{\partial \bar{x}_h} + \bar{v}_h \frac{\partial \bar{v}_h}{\partial \bar{y}_h} = -\frac{\partial \bar{P}_h}{\partial \bar{y}_h} + \frac{1}{Re_h}\left(\frac{\partial^2 \bar{v}_h}{\partial \bar{x}_h^2} + \frac{\partial^2 \bar{v}_h}{\partial \bar{y}_h^2}\right)$$ (4)

$$\left(\bar{u}_h \frac{\partial \bar{T}_h}{\partial \bar{x}_h} + \bar{v}_h \frac{\partial \bar{T}_h}{\partial \bar{y}_h}\right) = \frac{1}{Re_h\,Pr_h}\left(\frac{\partial^2 \bar{T}_h}{\partial \bar{x}_h^2} + \frac{\partial^2 \bar{T}_h}{\partial \bar{y}_h^2}\right)$$ (5)

$$\left(\bar{u}_h \frac{\partial \bar{w}_s}{\partial \bar{x}_h} + \bar{v}_h \frac{\partial \bar{w}_s}{\partial \bar{y}_h}\right) = \frac{1}{Re_h\,Sc}\left(\frac{\partial^2 \bar{w}_s}{\partial \bar{x}_h^2} + \frac{\partial^2 \bar{w}_s}{\partial \bar{y}_h^2}\right)$$ (6)

where the Reynolds, Prandtl and Schmidt numbers of the hot solution are, respectively,

$$Re_h = \frac{\rho_S u_{hi} d_h}{\mu_S}, \quad Pr_h = \frac{\mu_S c_{p_S}}{k_s}, \quad Sc_h = \frac{\nu_S}{D_S}$$ (7)

2.2. The membrane domain

The temperature difference between the hot and cold faces of the membrane is the driving force for evaporation of the water at the hot side, the flow of the produced vapor through the membrane pores, and its flow through the air/vapor gap to condense and form condensate (f) at the cooling plate (p) where its temperature is lower than the water vapor saturation temperature. In this analysis it is assumed that the diffusion of noncondensables gases from the feed solution across the membrane can be neglected, as it is very small compared with the water vapor flux.

The transport of the vapor through the membrane can be modeled by the molecular diffusion mechanism when the pore size of the membrane is in the micrometer range, which

is much bigger than the molecular mean free path of water vapor. The molecular diffusion model has been successfully applied to MD by various researchers (cf. [21–24]).

Stefan's law can be employed to model the permeate flux diffusion in the membrane at any location *x* along the membrane,

$$J_v(x) = K\Delta P_v$$ (8)

The vapor pressures (P_v) were calculated using the Antoine equation

$$\ln P_v = A_1 - \frac{A_2}{T_{h,m} - A_3}$$ (9)

where $A_1 = 16.2620$, $A_2 = 3799.89$, and $A_3 = -226.35$, P_v in Pa, $T_{h,m}$ is in °C. The validity of this equation was checked by comparison to the steam tables, and was found to be accurate to better than 0.4% within the 40–80 °C temperature range studied in this paper and K is the permeability of the membrane, defined (when air is present) as (cf. [18])

$$K = \frac{\varepsilon D_{v/a} M_v P_T}{\chi \delta_m P_{a,avg} R_u T_{avg,m}}$$ (10)

where ε (porosity), and χ (tortuosity), are membrane geometry parameters, $D_{v/a}$ is the diffusion coefficient of the vapor through the air, $P_{a,avg}$ is the average partial pressure of the air calculated by using Eqs. (9) and (11), P_T the total (air + vapor) pressure, and

$$T_{avg,m} = \frac{T_{hm} + T_{mg}}{2}$$ (11)

The effect of the presence of the salt in the solution on the vapor pressure at the hot surface of the membrane side has been accounted for by using the empirical correlation for the boiling point elevation in [25]. Raoult's Law can be used for the same purpose and its' mathematical expression is much simpler, but it is correct only for very dilute solutions. When using Raoult's Law, the vapor pressure at the hot side of the membrane (P_{hm}) is expressed as

$$P_{hm} = (1 - c_{s,hm})P_v(T_{hm})$$ (12)

The error incurred when it is used in place of the empirical correlation was calculated and is shown in Section 5.2.

The total sensible heat flux is transferred from the hot surface of the membrane to the condensation surface by two different parallel routes. One is by heat conduction across the membrane material and the air gap (Q_C) while the other is by the mass transfer of the vapor (Q_v)

$$Q_s = Q_v + Q_C$$ (13)

Using the analogy between heat and electricity, this heat flux can also be expressed as

$$Q_s = \frac{T_{hm} - T_{mg}}{R_{mT}}$$ (14)

where (R_{mT}) is the total heat transfer resistance in the membrane that can be expressed as

$$R_{mT} = \frac{R_m R_v}{(R_m + R_v)} \tag{15}$$

where the heat transfer resistance of the solid part of the membrane is

$$R_m = \frac{\delta_m}{k_{em}} \tag{16}$$

and the heat transfer resistance of the vapor flow through the membrane pores is

$$R_v = \frac{1}{J_v C_p} \tag{17}$$

The sensible heat transferred by vapor flow in the membrane is negligibly smaller than that by heat conduction ($R_v \gg R_m$). For example, for a typical permeate flux of 3×10^{-3} kg/m^{2}s, and a typical membrane thickness of 2×10^{-4} m, a simple calculation using Eqs. (16) and (17) shows that the ratio of the resistance due to conduction of the membrane material to that due to the vapor flow, $(R_m/R_v) = 0.003$. The thermal resistance of the membrane, Eq. (15), can thus be expressed as

$$R_{mT} = R_m = \frac{\delta_m}{k_{em}} \tag{18}$$

where

$$k_{em} = \varepsilon k_a + (1 - \varepsilon)k_m \tag{19}$$

where k_m, and k_a are the thermal conductivity of the membrane material, and the air, respectively.

2.3. The air/vapor gap domain

The vapor flow from the cold side of the membrane (interface mg in Fig. 1) to the condensation surface (fg) through the air gap (g) is affected by natural convection in the air gap. This natural convection takes place because of the temperature difference, $(T_{mg} - T_{gp})$, between these two surfaces, and its direction and intensity depend on the orientation of the air gap relative to the gravity vector. The relative importance of the natural convection is proportional to the Rayleigh number (Ra) (cf. [26]).

$$Ra \equiv \frac{g\beta\Delta T_g \delta_g^3}{\nu_a \alpha_a} \tag{20}$$

where ΔT_g is the temperature difference between the air gap hot and cold side, g is the gravitational acceleration, β is the thermal expansion coefficient, δ_g is the width of the air gap, and ν_a and α_a are the kinematics viscosity and thermal diffusivity of the air, respectively. It is of interest to know whether the natural convection is significant enough to be considered in AGMD analysis. For $\Delta T_g = 40\,°C$, and $\delta_g = 3$ mm (typical to AGMD), $Ra = 85.0$. For $Ra < 1000$, natural convection is negligible relative to heat conduction across the gap (cf. [27])

and thus heat transfer only by conduction across the gap was assumed in our study.

The thermal resistances of the air/vapor gap (R_g) can be expressed as

$$R_g = \frac{R_v R_a}{R_v + R_a} \tag{21}$$

where R_a and R_v represent the resistance to the conductive heat transfer, and the resistance to the convective heat transfer, respectively, and where

$$R_a = \frac{\delta_g - \delta_f}{k_a} \tag{22}$$

2.4. The condensate film

As the water vapor condenses on the cooling plate, it forms a condensate, and without special treatment, the condensation would be filmwise. This condensate film forms a heat transfer resistance that can be expressed as

$$R_f = \frac{\delta_f}{k_f} \tag{23}$$

with the assumption, verified below, that the heat convected with the gravitational flow of the condensate film is negligible as compared with the conduction across it.

The condensate film thickness (δ_f) can be calculated as follows. The amount of condensate added between x and $x + dx$ is (cf. [28])

$$d\dot{m}_f = \frac{\rho_f(\rho_f - \rho_v)g\delta_f^2 d\delta_f}{\mu_f} \tag{24}$$

which can also be expressed as

$$d\dot{m}_f = J_v(x)dx \tag{25}$$

Combining Eqs. (24) and (25), integrating the resulting expression, and solving for the condensate thickness at any x position, the condensate film thickness as a function of x is

$$\delta_f(x) = \left(\frac{3\mu_f \int_0^x J_v(x)dx}{g\rho_f(\rho_f - \rho_v)} \right)^{1/3} \tag{26}$$

To estimate whether one can assume one dimensional (y-direction) heat transfer in the film, we examine the ratio of the conductive heat flux across (y) the film to that carried by the film gravitational flow (in the x-direction). The conductive heat flux across the film can be calculated using

$$Q_{c,f} = k_f \frac{T_{gf} - T_{fp}}{\delta_f} \tag{27}$$

In steady state the entire vapor flux J is condensed and is drained gravitationally as condensate, and thus the heat carried with the film flow is

$$Q_{cov,f} = Jh_f = \rho_f u_f \delta_f h_f \tag{28}$$

where u_f is the average velocity of the film drainage. The ratio of these quantities, Eqs. (27) and (28), is

$$\frac{Q_{C,f}}{Q_{cov,f}} = \frac{k_f(T_{gf} - T_{fp})}{Jh_f\delta_f} = \frac{k_f(T_{gf} - T_{fp})}{\rho_f h_f u_f \delta_f^2} \quad (29)$$

This shows that the ratio of the conductive to the convective heat transfer is function of the second power of the thickness of condensate film, and thus convective heat transfer can be neglected if the condensate film is small. Calculating the properties at 25 °C and using a typical value of $J = 3 \times 10^{-3}$ kg/m²s and $x = 0.2$ m, Eq. (26) produces $\delta_f = 8.6 \times 10^{-5}$ m. Using Eq. (29), the ratio of conductive to drainage heat flows is 302, and thus the drainage heat flow can be neglected, justifying assumption of one-dimensional heat transfer.

2.5. The cooling plate

Both the heat conducted through the air/vapor gap and the heat released by vapor condensation are then transferred by heat conduction through the cooling plate and further convected to the cooling fluid. The thermal resistance of the cooling plate can be expressed as

$$R_p = \frac{\delta_p}{k_p} \quad (30)$$

where δ_p is the cooling plate thickness, and k_p its thermal conductivity.

The temperature at the cold side of the membrane, T_{mg}, can be calculated by balancing the sensible heat transferred through the membrane and that through the air/vapor gap. Toward this end, the sensible heat flux transferred from the hot to the cold side of the membrane

$$Q_s = \frac{T_{hm} - T_{mg}}{R_m} \quad (31)$$

where R_m is calculated by Eq. (16), and the sensible heat flux transferred from the cold side of the membrane (mg) to the cooling plate cold side (pc) can be also expressed by

$$Q_s(x) = \frac{T_{mg} - T_{pc}}{R_s - R_m} \quad (32)$$

where R_s

$$R_s = R_m + R_g + R_f + R_p \quad (33)$$

where R_m is calculated by Eq. (16), R_g is calculated by Eq. (21), R_f is calculated by Eq. (23), and R_p is calculated by Eq. (30).

Combining Eqs. (31) and (32) and solving for T_{mg}, we have

$$T_{mg} = \frac{R_s - R_m}{R_s} T_{hm} + \frac{R_m}{R_s} T_{pc} \quad (34)$$

Similarly, the temperatures T_{gf} and T_{fp} can be expressed as

$$T_{gf} = \frac{R_f + R_p}{R_s} T_{hm} + \frac{R_m + R_g}{R_s} T_{pc} \quad (35)$$

$$T_{fp} = \frac{R_p}{R_s} T_{hm} + \frac{R_s - R_p}{R_s} T_{pc} \quad (36)$$

At any location x, the conductive heat flux is

$$Q_C = k_{me} \frac{T_{hm} - T_{mc}}{\delta_m} \quad (37)$$

and the latent heat flux is

$$Q_L = J_v h_{fg} \quad (38)$$

So the total heat flux is

$$Q_T = Q_L + Q_C \quad (39)$$

2.6. The cold solution region

The continuity, momentum, and energy equations in the cooling solution are normalized by using the dimensionless variables

$$\begin{aligned}
&\bar{x}_c = \frac{x_c}{d_h}, \quad \bar{y}_c = \frac{y_c}{d_h} \\
&\bar{u}_c = \frac{u_c}{u_{ci}}, \quad \bar{v}_c = \frac{v_c}{u_{ci}}, \\
&\bar{P}_c = \frac{P_c}{\rho_S u_{ci}^2}, \\
&\bar{T}_c = \frac{T_c - T_{ci}}{T_{hi} - T_{ci}}
\end{aligned} \quad (40)$$

and the equations are

$$\frac{\partial \bar{u}_c}{\partial \bar{x}_c} + \frac{\partial \bar{v}_c}{\partial \bar{y}_c} = 0 \quad (41)$$

$$\bar{u}_c \frac{\partial \bar{u}_c}{\partial \bar{x}_c} + \bar{v}_c \frac{\partial \bar{u}_c}{\partial \bar{y}_c} = -\frac{\partial \bar{P}_c}{\partial \bar{x}_c} + \frac{1}{Re_c}\left(\frac{\partial^2 \bar{u}_c}{\partial \bar{x}_c^2} + \frac{\partial^2 \bar{u}_c}{\partial \bar{y}_c^2}\right) \quad (42)$$

$$\bar{u}_c \frac{\partial \bar{v}_c}{\partial \bar{x}_c} + \bar{v}_c \frac{\partial \bar{v}_c}{\partial \bar{y}_c} = -\frac{\partial \bar{P}_c}{\partial \bar{y}_c} + \frac{1}{Re_c}\left(\frac{\partial^2 \bar{v}_c}{\partial \bar{x}_c^2} + \frac{\partial^2 \bar{v}_c}{\partial \bar{y}_c^2}\right) \quad (43)$$

$$\left(\bar{u}_c \frac{\partial \bar{T}_c}{\partial \bar{x}_c} + \bar{v}_c \frac{\partial \bar{T}_c}{\partial \bar{y}_c}\right) = \frac{1}{Re_c Pr_c}\left(\frac{\partial^2 \bar{T}_c}{\partial \bar{x}_c^2} + \frac{\partial^2 \bar{T}_c}{\partial \bar{y}_c^2}\right) \quad (44)$$

where the Reynolds and Prandtl numbers of the cold solution are defined, respectively, as,

$$Re_c = \frac{\rho_S u_{ci} d_c}{\mu_S}, \quad Pr_c = \frac{\mu_S c_{p_S}}{k_S} \quad (45)$$

The equation of species for the cold solution is not included in the model because there is no mass transport in the cold channel.

2.7. The model boundary conditions

In dimensionless form, by using the variables in Eq. (1) the boundary conditions become:

Inlet interfaces (hi, ci)

$$\bar{u}_h = 1, \quad \bar{v}_h = 0, \quad \bar{T}_h = 1, \quad \bar{w}_s = 1 \tag{46}$$

$$\bar{u}_c = 1, \quad \bar{v}_c = 0, \quad \bar{T}_c = 0 \tag{47}$$

Center of the channel interfaces (hc,cc)

$$\frac{\partial \bar{u}_h}{\partial \bar{y}_h} = 0; \quad \bar{v}_h = 0; \quad \frac{\partial \bar{T}_h}{\partial \bar{y}_h} = 0; \quad \frac{\partial \bar{w}_s}{\partial \bar{y}_h} = 0 \tag{48}$$

$$\frac{\partial \bar{u}_c}{\partial \bar{y}_c} = 0; \quad \bar{v}_c = 0; \quad \frac{\partial \bar{T}_c}{\partial \bar{y}_c} = 0; \quad \frac{\partial \bar{w}_s}{\partial \bar{y}_c} = 0 \tag{49}$$

Outlet of channels interfaces (hoe,coe)

$$\bar{P}_h = 0 \tag{50}$$

$$\bar{P}_c = 0 \tag{51}$$

Outlet of the channel Interfaces (ho,co)

The convective term is much larger than the conductive term in the energy equation and the diffusive term in the diffusion equation[1] at the hot solution channel exit,

$$(u_{hi}\rho_S Cp_S \bar{u}_h \bar{T}_h + k_S \Delta \bar{T}_h) \cdot \vec{n} \approx u_{hi}\rho_S Cp_S \bar{u}_h \bar{T}_h \cdot \vec{n} \tag{52}$$

$$(u_{hi}\bar{u}_h \bar{w}_s + D_S \Delta \bar{w}_s) \cdot \vec{n} \approx u_{hi}\bar{u}_h \bar{w}_s \cdot \vec{n} \tag{53}$$

$$(u_{ci}\rho_S Cp_S \bar{u}_c \bar{T}_c + k_S \Delta \bar{T}_c) \cdot \vec{n} \approx u_{hi}\rho_S Cp_S \bar{u}_c \bar{T}_c \cdot \vec{n} \tag{54}$$

where $\vec{n}$ is the unit vector normal to the boundary interface.

Membrane hot surface interface (hm)

$$\bar{u}_h = 0 \tag{55}$$

$$\bar{v}_h = \frac{J_v}{u_{hi}\rho_s} \tag{56}$$

$$-k_S \frac{d\bar{T}_h}{d\bar{y}_h} = \frac{d_h(Q_C + J_v h_{fg})}{T_{hi} - T_{ci}} \tag{57}$$

$$\frac{D_S}{d_h} \frac{\partial \bar{w}_s}{\partial \bar{y}_h} = \frac{J_v}{w_{s,i}\rho_S} \tag{58}$$

Cooling plate cold side interface (pc),

$$\bar{u}_c = 0 \tag{59}$$

$$\bar{v}_c = 0 \tag{60}$$

$$-k_S \frac{d\bar{T}_c}{d\bar{y}_c} = \frac{d_h(k_{em}\nabla T_m + J_v h_{fg})}{T_{hi} - T_{ci}} \tag{61}$$

---

[1] To verify these assumptions, it was calculated for typical conditions that for the hot solution the convective term $\rho_S Cp_S u_c T = 3.95 \times 10^5$ W m^{-2} °C^{-1}, and the conductive term $(k_S) dT/dx = 3.38 \times 10^{-4}$ W m^{-2} °C, and for the cold solution $\rho_S Cp_S u_h T = 2.15 \times 10^4$ W m^{-2} °C^{-1}, and $(k_S) dT/dx = 5.64 \times 10^{-4}$ W m^{-2} °C^{-1}. For the equation of species, the convective and diffusive terms are 0.1335 and 1.02×10^{-9} W m^{-2} °C^{-1}, respectively.

3. Process parameters

The parameters to be evaluated in this work include the averaged permeate flux, the conductive heat transfer, the total heat transfer, the process thermal efficiency.

The averaged permeate flux is obtained by integrating Eq. (8) over the length of the membrane and dividing by the membrane length (l_m)

$$J = \frac{1}{l_m} \int_0^{l_m} J_v(x)dx \tag{62}$$

by integrating Eq. (37), the x-averaged conduction heat flux is

$$\tilde{Q}_C = \frac{1}{l_m} \int_0^{l_m} Q_C(x)dx \tag{63}$$

by integrating Eq. (38), the x-averaged latent heat flux is

$$\tilde{Q}_L = \frac{1}{l_m} \int_0^{l_m} Q_L(x)dx \tag{64}$$

and by integrating Eq. (39), the total heat transfer is

$$\tilde{Q}_T = \frac{1}{l_m} \int_0^{l_m} Q_T(x)dx \tag{65}$$

The process thermal efficiency can be defined as

$$\eta_t = \frac{\tilde{Q}_L}{\tilde{Q}_T} \tag{66}$$

where the numerator is the heat used for the production of the distillate.

4. Method of solution, grid independence, and validation

Eqs. (2)–(6) and (41)–(44) constitute nine second-order partial differential equations in two dimensions, with nine unknowns ($\bar{u}_h, \bar{v}_h, \bar{P}_h, \bar{T}_h, \bar{w}_s, \bar{u}_c, \bar{v}_c, \bar{P}_c, \bar{T}_c$). This set of equations was solved together with the needed 36 boundary conditions described by Eqs. (46)–(61). These include six boundary conditions for $\bar{u}_h$, six boundary conditions for $\bar{v}_h$, six boundary conditions for $\bar{u}_c$, six boundary conditions for $\bar{v}_c$, four boundary conditions for $\bar{T}_h$, four boundary conditions for $\bar{T}_c$, and four boundary conditions for $\bar{w}_s$. The Femlab finite element program [29] was used for the solution. It is noteworthy that the model described by this set of equations is valid for most solutions, where Stefan's law with molecular diffusion through the membrane can be assumed (the conditions for this are described in Section 2.2), once the specific properties of the solutions and the range of parameters are taken into account. It was, however, solved and validated here only for aqueous NaCl solutions as described.

The base-case model main dimensions are $d_h = 2$ mm, $l_m = 0.2$ m, $\delta_m = 4 \times 10^{-4}$ m, $\delta_g = 2$ mm.

While the solution properties change with temperature and concentration, they were assumed in our computations to be

constant, at the mid range of each run, with the following justification (1) the temperature variations are relatively small, with the thermal conductivity variation over that range being only 1%, of specific heat 0.1%, and of density 0.6%. The variation of thee viscosity is about 10%, but it was still assumed that the influence of this variation on the sought results is negligible because experimental work [21] has shown that the effect of 30 wt.% sucrose is less than that caused by 25% wt.% NaCl under the same conditions, which implies that the effect of the viscosity on the flux is less than that of the concentration of salt, which has been shown to have a very small effect on the flux anyway, (2) the physical properties are affected little by the concentration of NaCl: for a three-fold increase in the concentration, from 20,000 to 60,000 ppm, the thermal conductivity and specific heat are almost unaffected; density increased by 2.2%, and viscosity by 4.5%. The diffusion coefficient of vapor through air [$D_{v/a}$, Eq. (10)] varies by at most 4.5% within that studied range of temperatures and pressures [30]. Considering the general modeling error, we believe therefore that the additional effort of computing temperature and concentration dependent properties would have made the computation longer and more difficult yet yielded little improvement.

The physical properties of the aqueous NaCl solutions used in this study were calculated from temperature and concentration dependent correlations: enthalpy (heat capacity) [31], viscosity [32], density [33], and thermal conductivity [34].

A grid-dependence analysis of the method of solution was performed. The number of elements is chosen to be 13,258 because further refinement of the mesh to 29,926 elements produced just a 0.03% difference in J.

To ensure that the numerical solution is not affected adversely by the specification of the inlet conditions to the hot and cold liquid flow channels, the sensitivity of the solution to the location where the inlet boundary conditions were specified was investigated. Comparing the velocity distributions for specifying the inlet at a distance of $A_h/2$ (the aspect ratio, $A_h = 100$) upstream of the channels' inlets (Fig. 1), and for specifying them at the inlet itself ($x = 0$), has shown no discernible differences.

The computed results were validated by comparison with Banat's [6] AGMD experimental ones, and were found to be in very good agreement, within about 5%, as shown in Fig. 2.

5. Results and discussion

The analysis is made for the inlet temperature of the feed solution (T_{hi}) in the range 40–80 °C computed at 5 °C increments, hot solution inlet sodium chloride concentrations of 20,000–50,000 ppm at 5000 increments, feed and cold solutions inlet velocities (u_{hi}, u_{ci}) of 0.1–0.3 m/s ($Re_h = 1393$–464, $Re_c = 583$–193), at 0.04 m/s increments, cooling solution inlet temperatures (T_{ci}) of 5–45 °C at 5 °C increments, air/vapor gap widths (δ_g) of 1–5 mm at
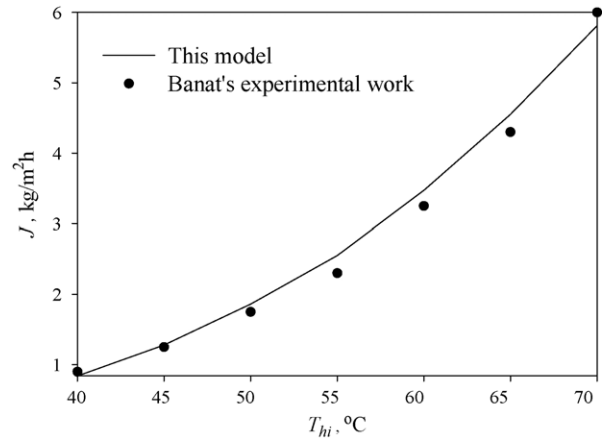

Fig. 2. The effect of the temperature on the permeate flux as in this study, in comparison with Banat's AGMD experiments [6]. $T_{ci} = 20$ °C, $u_{hi} = 0.1$ m/s ($Re_h = 464$), $d_h = 2$ mm, $l_m = 0.2$ m, $\delta_m = 6 \times 10^{-4}$ m, $\delta_g = 3.5$ mm, $u_{ci} = 0.1$ m/s, $\varepsilon = 0.75$.

1 mm increments, membrane thermal conductivities (k_m) of 0.05–0.3 W m^{-1} K^{-1} at 0.05 W m^{-1} K^{-1} increments, and membrane porosities (ε_m) of 0.74, 0.78, and 0.84.

The velocity distributions in the hot solution along $\bar{x}_h$ in the hot channel and of the cold solution along $\bar{x}_c$ in the cold channel are shown in Fig. 3 at $\bar{x}_h$ and $\bar{x}_c$ = 10, 20, 40, and 80. Both flows show the boundary layers growth along the respective channels, with the boundary layer thickness increasing by approximately two-fold from $\bar{x} = 10$ to 80. Similarly, the temperature and concentration distributions along the hot channel and the temperature distributions in the cold channel are shown in Fig. 4. The boundary layer grows at a faster rate near the entrance of the channels (noting the growth between
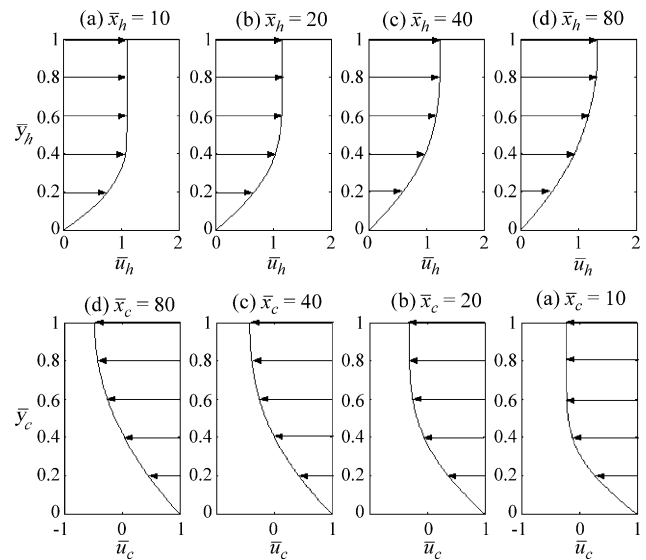

Fig. 3. Velocity distributions in the hot and cold channels at (a) $\bar{x}_h = 10$, (b) $\bar{x}_h = 20$, (c) $\bar{x}_h = 40$, (d) $\bar{x}_h = 80$. $u_{hi} = 0.2$ m/s ($Re_h = 928$), $T_{hi} = 70$ °C, $w_{si} = 0.025$, $T_{ci} = 20$ °C $d_h = 0.002$ m, $l_m = 0.2$ m, $\delta_m = 4 \times 10^{-4}$ m, $\chi = 1.5$, $k_m = 0.2$ W m^{-1} K^{-1}, $\varepsilon = 0.78$, $\delta_g = 2 \times 10^{-3}$ m, $k_p = 60$ W m^{-1} K^{-1}, $\delta_p = 1.5 \times 10^{-3}$ m, $u_{ci} = 0.2$ m/s ($Re_c = 386$), $d_c = 0.002$ m.
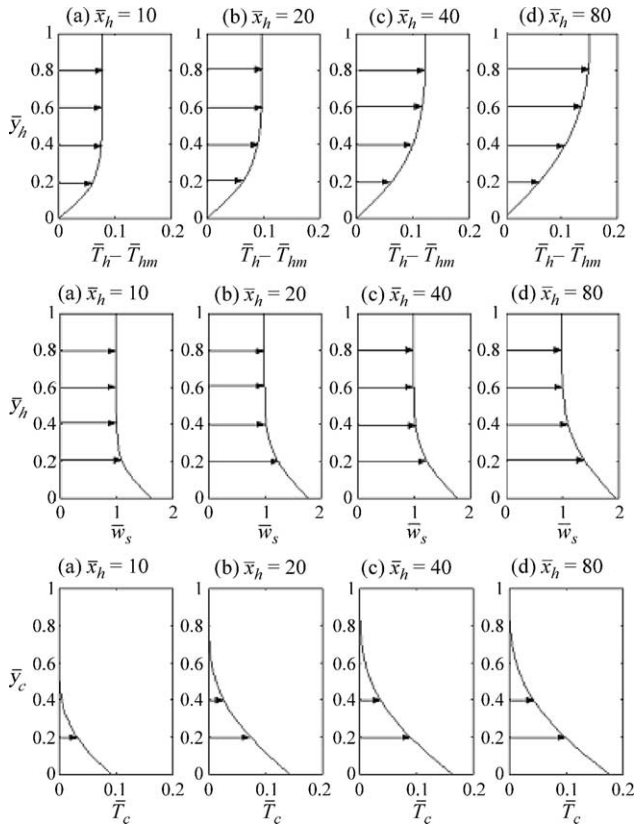
Fig. 4. Temperature and concentration distributions in the hot and cold channels at different location of the hot and cold channels. $u_{hi} = 0.2$ m/s ($Re_h = 928$), $T_{hi} = 70\,°C$, $w_{si} = 0.025$, $T_{ci} = 20\,°C$ $d_h = 0.002$ m, $l_m = 0.2$ m, $\delta_m = 4 \times 10^{-4}$ m, $\chi = 1.5$, $k_m = 0.2\,\mathrm{Wm^{-1}\,K^{-1}}$, $\varepsilon = 0.78$, $\delta_g = 2 \times 10^{-3}$ m, $k_p = 60\,\mathrm{Wm^{-1}\,K^{-1}}$, $\delta_p = 1.5 \times 10^{-3}$ m, $u_{ci} = 0.2$ m/s ($Re_c = 386$), $d_c = 0.002$ m.

$\bar{x}_h = 10$ and 40, in comparison with that between $\bar{x}_h = 40$ and 80 in the hot channel, and between $\bar{x}_c = 10$ and 40 as opposed to that between $\bar{x}_c = 40$ and 80 in the cold channel). This implies that the heat transfer coefficient, and thus the local permeate flux, are (as expected) higher near the hot channel entrance.

Fig. 5 shows the temperature profile across the AGMD cell at the entrance of the hot ($\bar{x}_h = 0$) and cold ($\bar{x}_c = 0$) channels and at $\bar{x}_h = \bar{x}_c = 50$. The temperature changes are indicative of the heat transfer processes, including the boundary layer behavior in the hot and cold channels. The temperature drop is highest in the air gap domain as it constitutes the biggest thermal resistance. A quantitative analysis and the sensitivity of the process parameters are presented below.

5.1. The effect of inlet temperature of the hot and cold solutions

Fig. 6 shows the effect of the hot and cold solution inlet temperatures on the permeate flux. The permeate flux is affected greatly by the hot solution inlet temperature, and to smaller extent by the inlet temperature of the cold solution.
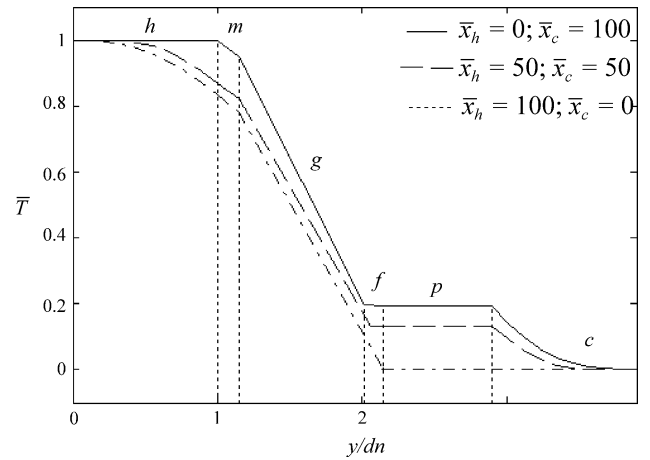

Fig. 5. The temperature profile across the AGMD unit. The letters indicate the different domains, see Fig. 1. $T_{hi} = 70\,°C$. $T_{ci} = 20\,°C$, $u_{hi} = 0.1$ m/s ($Re_h = 464$), $w_{si} = 0.025$, $d_h = 0.002$ m, $l_m = 0.2$ m, $\delta_m = 4 \times 10^{-4}$ m, $\chi = 1.5$, $k_m = 0.2\,\mathrm{Wm^{-1}\,K^{-1}}$, $\varepsilon = 0.78$, $\delta_g = 2$ mm, $k_p = 60\,\mathrm{Wm^{-1}\,K^{-1}}$, $\delta_p = 1.5 \times 10^{-3}$ m, $u_{ci} = 0.1$ m/s ($Re_c = 193$), $d_c = 0.002$ m.

Increasing T_{hi} from 40 to 80 °C increases the flux nine-fold. For the same temperature change, decreasing the temperature of the cold solution, T_{ci}, from 45 to 5 °C, increases the flux by only about two-fold. The hot solution temperature has a greater influence because of the exponential increase of the partial pressure of the vapor with the temperature, so the driving force is greater at higher temperatures.

Fig. 7 shows the conductive heat transfer as a function of the inlet temperature of the hot and cold solutions. Increasing T_{hi} from 40 to 80 °C increases the heat transferred by con-
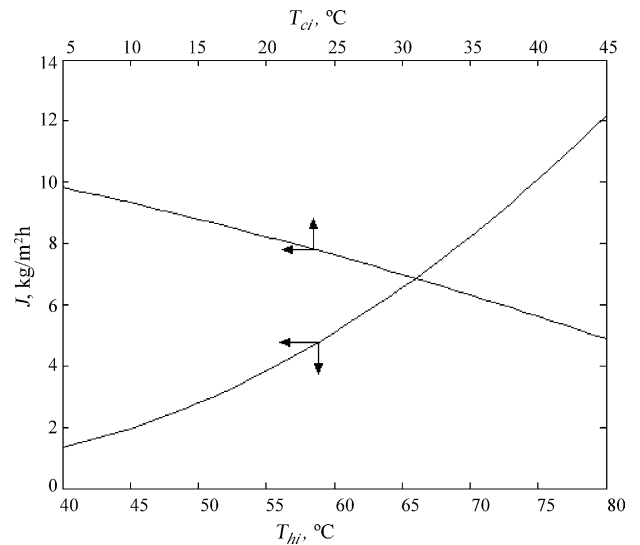

Fig. 6. The effect of the inlet temperature of the hot and cold solutions on the permeate flux. $T_{hi} = 70\,°C$ (when T_{ci} varies). $T_{ci} = 20\,°C$ (when T_{hi} varies), $u_{hi} = 0.1$ m/s ($Re_h = 464$), $w_{si} = 0.025$, $d_h = 0.002$ m, $l_m = 0.2$ m, $\delta_m = 4 \times 10^{-4}$ m, $\chi = 1.5$, $k_m = 0.2\,\mathrm{Wm^{-1}\,K^{-1}}$, $\varepsilon = 0.78$, $\delta_g = 2$ mm, $k_p = 60\,\mathrm{Wm^{-1}\,K^{-1}}$, $\delta_p = 1.5 \times 10^{-3}$ m, $u_{ci} = 0.1$ m/s ($Re_c = 193$), $d_c = 0.002$ m.
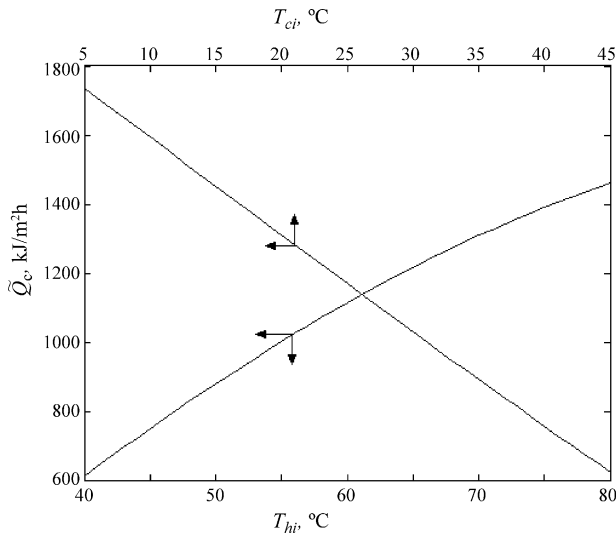
Fig. 7. The effect of the inlet temperature of the hot and cold solutions on the conductive heat transfer flux. $T_{hi} = 70\,^{\circ}C$ (when T_{ci} varies), $T_{ci} = 20\,^{\circ}C$ (when T_{hi} varies), $u_{hi} = 0.1$ ($Re_h = 464$) m/s, $w_{si} = 0.025$, $d_h = 0.002$ m, $l_m = 0.2$ m, $\delta_m = 4 \times 10^{-4}$ m, $\chi = 1.5$, $k_m = 0.2\,Wm^{-1}\,K^{-1}$, $\varepsilon = 0.78$, $\delta_g = 2$ mm, $k_p = 60\,Wm^{-1}\,K^{-1}$, $\delta_p = 1.5 \times 10^{-3}$ m, $u_{ci} = 0.1$ m/s ($Re_c = 193$), $d_c = 0.002$ m.

Fig. 9. Comparison of the effect of the hot solution inlet concentration to that of its inlet temperature, on the permeate flux. $T_{hi} = 70\,^{\circ}C$ (when w_{si} varies), $T_{ci} = 20\,^{\circ}C$, $u_{hi} = 0.1$ ($Re_h = 464$), m/s, $w_{si} = 0.025$ (when T_{hi} varies), $d_h = 0.002$ m, $l_m = 0.2$ m, $\delta_m = 4 \times 10^{-4}$ m, $\chi = 1.5$, $k_m = 0.2\,Wm^{-1}\,K^{-1}$, $\varepsilon = 0.78$, $\delta_g = 2$ mm, $k_{pl} = 60\,Wm^{-1}\,K^{-1}$, $\delta_p = 1.5 \times 10^{-3}$ m, $u_{ci} = 0.1$ m/s ($Re_c = 193$), $d_c = 0.002$ m.

duction by about 2.4-fold. For the same temperature range, decreasing T_{ci} from 45 to $5\,^{\circ}C$, increases $\tilde{Q}_C$ by 2.8-fold. Therefore, lowering the inlet cold solution temperature results in slightly more heat transfer by conduction (i.e., heat loss) than when increasing the inlet hot solution temperature.

Fig. 8 shows the effect of the hot and cold solution inlet temperatures on the thermal efficiency. The thermal
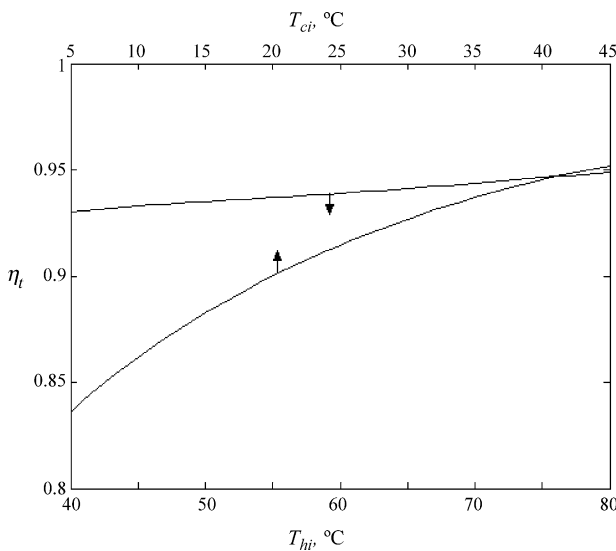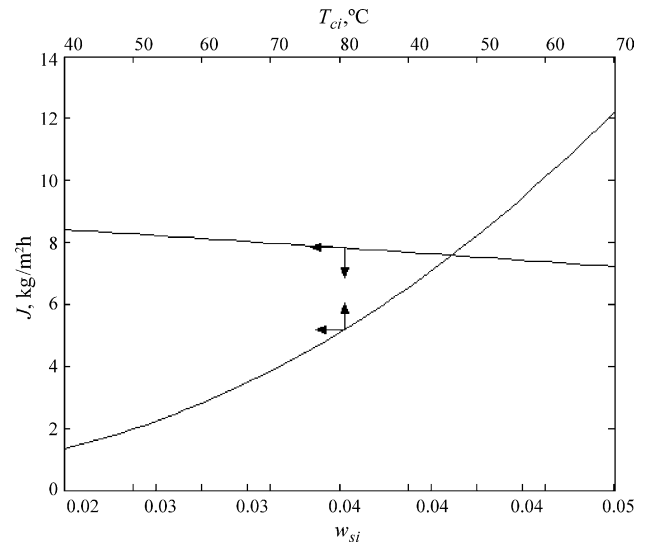

Fig. 8. The effect of the inlet temperature of the hot and cold solutions on the process thermal efficiency, η_t. $T_{hi} = 70\,^{\circ}C$ (when T_{ci} varies), $T_{ci} = 20\,^{\circ}C$ (when T_{hi} varies), $u_{hi} = 0.1$ m/s ($Re_h = 464$), $w_{si} = 0.025$, $d_h = 0.002$ m, $l_m = 0.2$ m, $\delta_m = 4 \times 10^{-4}$ m, $\chi = 1.5$, $k_m = 0.2\,Wm^{-1}\,K^{-1}$, $\varepsilon = 0.78$, $\delta_g = 2$ mm, $k_p = 60\,Wm^{-1}\,K^{-1}$, $\delta_p = 1.5 \times 10^{-3}$ m, $u_{ci} = 0.1$ m/s ($Re_c = 193$), $d_c = 0.002$ m.

efficiency increases by about 12% as T_{hi} is increases from 40 to $80\,^{\circ}C$ because the rate of increase of Q_L is higher than that of Q_C (Eqs. (39) and (66)). The reduction of T_{ci} causes the heat efficiency to slightly drop. Decreasing T_{ci} from 45 to $5\,^{\circ}C$, decreases η_t by 2.5%.

Increasing the inlet temperature of the hot solution thus does not only increase the permeate flux but also improves the thermal efficiency. To lesser extent, lowering the inlet temperature of the cold solution will improve the permeate flux, but will slightly decrease the heat efficiency.

5.2. The effect of the inlet concentration of the hot solution

Fig. 9 shows the effect of the inlet concentration of the hot solution (w_{si}), in comparison with the effect of its inlet temperature (T_{hi}), on the permeate flux (J). It can be seen that the concentration of the inlet hot solution has a relatively small effect: increasing w_s from 0.02 (20,000 ppm) to 0.05 (50,000 ppm), at a constant temperature, reduces the permeate flux by only 16%. The moderate effect of solution concentration on the permeate flux is an advantage of MD over pressure-driven membrane processes, such as reverse osmosis, in which the concentration plays a significant role on the process, and makes it possible for MD to be used as a bottoming device to process RO brines for further fresh water production.

The heat transferred by conduction as a function of the hot solution concentration, in comparison with the effect of its inlet temperature (T_{hi}), is shown in Fig. 10. $\tilde{Q}_C$ increases very slightly (3%) with the increase of w_{si} from 0.02 (20,000 ppm) to 0.05 (50,000 ppm).
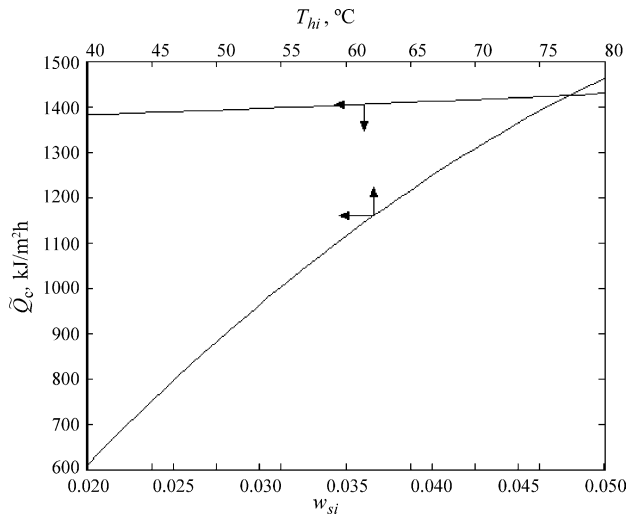
Fig. 10. Comparison of the effect of the hot solution inlet concentration to that of its inlet temperature, on the conductive heat transfer flux. $T_{hi} = 70\,^\circ$C (when w_{si} varies), $T_{ci} = 20\,^\circ$C, $u_{hi} = 0.1$ m/s ($Re_h = 464$), $w_{si} = 0.025$ (when T_{hi} varies), $d_h = 0.002$ m, $l_m = 0.2$ m, $\delta_m = 4 \times 10^{-4}$ m, $\chi = 1.5$, $k_m = 0.2\,\text{Wm}^{-1}\,\text{K}^{-1}$, $\varepsilon = 0.78$, $\delta_g = 2$ mm, $k_{pl} = 60\,\text{Wm}^{-1}\,\text{K}^{-1}$, $\delta_p = 1.5 \times 10^{-3}$ m, $u_{ci} = 0.1$ m/s ($Re_c = 193$), $d_c = 0.002$ m.

Fig. 11 shows the thermal efficiency η_t as a function of the inlet concentration of the hot solution, in comparison with the effect of its inlet temperature (T_{hi}). η_t is reduced by only 2% with the increase in w_{si} from 0.02 (20,000 ppm) to 0.05 (50,000 ppm).

It is noteworthy here to note that the effect of concentration on the boiling point elevation is computed in this study by an empirical correlation [26] developed for NaCl solu-
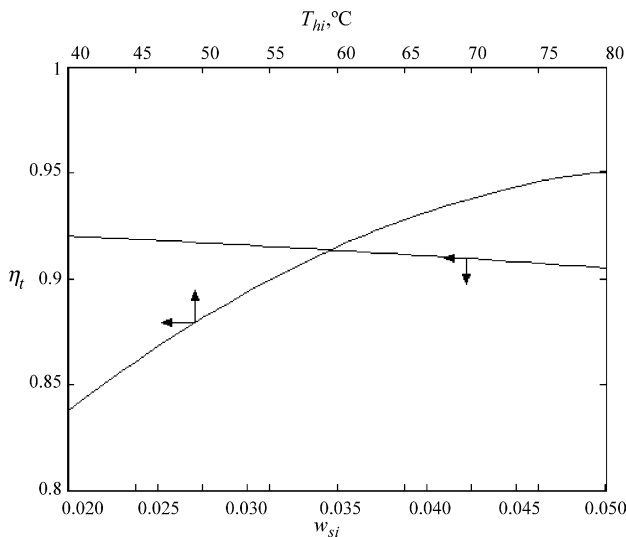

Fig. 11. Comparison of the effect of the hot solution inlet concentration to that of its inlet temperature, on the process thermal efficiency. $T_{hi} = 70\,^\circ$C (when w_{si} varies), $T_{ci} = 20\,^\circ$C, $u_{hi} = 0.1$ m/s ($Re_h = 464$), $w_{si} = 0.025$ (when T_{hi} varies), $d_h = 0.002$ m, $l_m = 0.2$ m, $\delta_m = 4 \times 10^{-4}$ m, $\chi = 1.5$, $k_m = 0.2\,\text{Wm}^{-1}\,\text{K}^{-1}$, $\varepsilon = 0.78$, $\delta_g = 2$ mm, $k_{pl} = 60\,\text{Wm}^{-1}\,\text{K}^{-1}$, $\delta_p = 1.5 \times 10^{-3}$ m, $u_{ci} = 0.1$ m/s ($Re_c = 193$), $d_c = 0.002$ m.
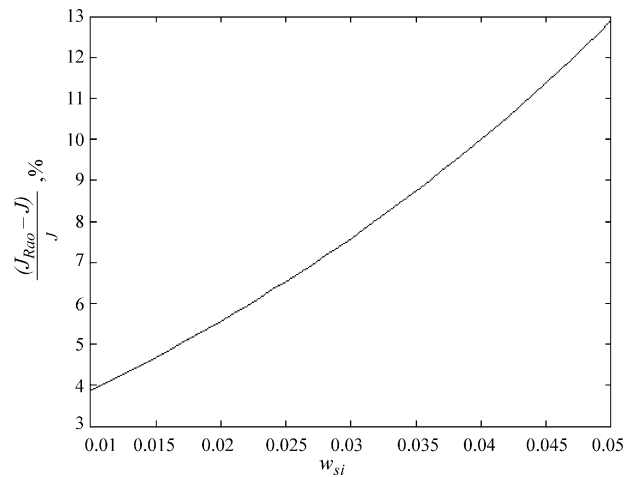

Fig. 12. The percentage error of the permeate flux as the effect of the concentration computed by using Raoult's law (J_{Rao}) to that computed by using the empirical correlation [26], (J). $T_{hi} = 70\,^\circ$C $T_{ci} = 20\,^\circ$C, $u_{hi} = 0.1$ m/s ($Re_h = 464$), $d_h = 0.002$ m, $l_m = 0.2$ m, $\delta_m = 4 \times 10^{-4}$ m, $\chi = 1.5$, $k_m = 0.2\,\text{Wm}^{-1}\,\text{K}^{-1}$, $\varepsilon = 0.78$, $\delta_g = 2$ mm, $k_{pl} = 60\,\text{Wm}^{-1}\,\text{K}^{-1}$, $\delta_p = 1.5 \times 10^{-3}$ m, $u_{ci} = 0.1$ m/s ($Re_c = 193$), $d_c = 0.002$ m.

tions of concentrations including the ones investigated in this study. This can also be done by using Raoult's law, which is mathematically much simpler, but correct only for solutions much weaker than seawater or typical brackish water. To estimate the error incurred by this assumption, computations were also conducted using Raoul's law, and the ratio of the permeate flux when Raoult's law is used over that when empirical correlation is used is shown in Fig. 12. It can be seen that using Raoult's law overestimates the permeate flux by just 4% at $w_{si} = 0.01$ (10,000 ppm), and by about 13% at $w_{si} = 0.05$ (50,000 ppm).

5.3. The effect of the inlet velocity of the hot and cold solutions

Fig. 13 shows the permeate flux (J) as a function of both the hot (u_{hi}) and the cold (u_{ci}) solutions inlet velocities. J increases with the increases of both velocities, and the effect of u_{hi} is greater than that of u_{ci}: for the same velocity magnitude increase from 0.1 to 0.3 m/s ($Re_h = 464$–1393, $Re_c = 193$–583), J increases by about 11% with u_{hi}, and only by 3% with u_{ci}. The improvement is because higher velocities reduce the y-direction temperature drop in the solutions thus effectively increasing the driving temperature difference, and that has a higher effect on the vapor pressure in the hot solution as discussed above.

The heat transferred by conduction as a function of inlet velocity of the hot and cold solutions is shown in Fig. 14. For the same velocity magnitude increase from 0.1 to 0.3 m/s, $\tilde{Q}_C$ changes very slightly with both u_{hi} and u_{ci}: it increases by about 3% with u_{hi} and 5% with u_{ci}.

The velocity affects the process by reducing the boundary layer thicknesses of the temperature and concentration of the hot and the temperature of the cold solutions (Fig. 15).
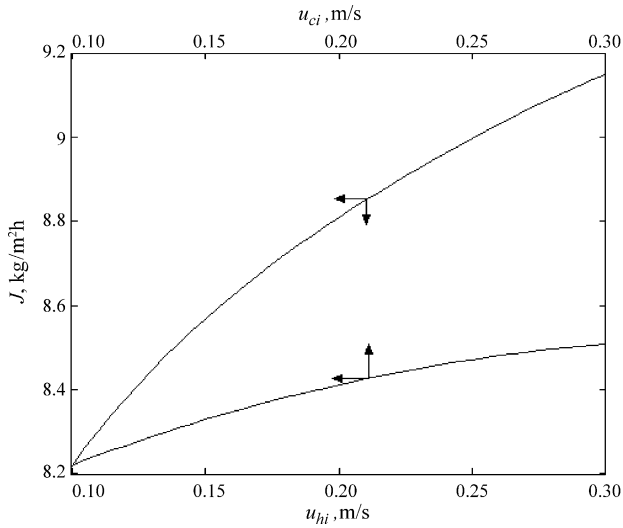
Fig. 13. The permeate flux as of function of inlet velocity of the hot (u_hi) and cold (u_ci) solutions. $T_\text{hi} = 70\,^\circ\text{C}$, $T_\text{ci} = 20\,^\circ\text{C}$, $w_\text{si} = 0.025$, $u_\text{hi} = 0.1$ (when u_ci varies) $Re_\text{h} = 464$, $d_\text{h} = 0.002\,\text{m}$, $l_\text{m} = 0.2\,\text{m}$, $\delta_\text{m} = 4 \times 10^{-4}\,\text{m}$, $k_\text{m} = 0.2\,\text{Wm}^{-1}\,\text{K}^{-1}$, $\chi = 1.5$, $\varepsilon = 0.78$, $\delta_\text{g} = 2\,\text{mm}$, $k_\text{p} = 60\,\text{Wm}^{-1}\,\text{K}^{-1}$, $\delta_\text{p} = 1.5 \times 10^{-3}\,\text{m}$, $u_\text{ci} = 0.1$ (when u_hi varies) $Re_\text{c} = 193$, $d_\text{c} = 0.002\,\text{m}$.

The upper row of Fig. 15 shows that upper level value of $\bar{T}_\text{h}$ becomes higher and closer to the membrane surface as the velocity increases from 0.1 to 0.3 m/s, second row shows that the concentration (w_si) becomes smaller and closer to the membrane, and the bottom row shows that $\bar{T}_\text{c}$ becomes smaller and closer to the cooling plate surface as u_ci increases from 0.1 to 0.3 m/s. The consequences of this is that the evaporation takes place at higher driving force with higher temperature, and less solution concentration, and thus produces higher permeate flux.
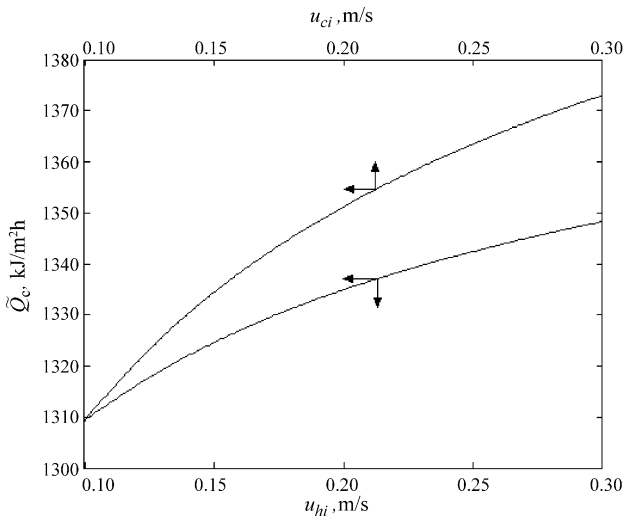

Fig. 14. The conduction heat transfer flux as a function of the hot (u_hi) and cold (u_ci) solution inlet velocities. $T_\text{hi} = 70\,^\circ\text{C}$, $T_\text{ci} = 20\,^\circ\text{C}$, $w_\text{si} = 0.025$, $u_\text{hi} = 0.1$ (when u_ci varies) $Re_\text{h} = 464$, $d_\text{h} = 0.002\,\text{m}$, $l_\text{m} = 0.2\,\text{m}$, $\delta_\text{m} = 4 \times 10^{-4}\,\text{m}$, $k_\text{m} = 0.2\,\text{Wm}^{-1}\,\text{K}^{-1}$, $\chi = 1.5$, $\varepsilon = 0.78$, $\delta_\text{g} = 2\,\text{mm}$, $k_\text{p} = 60\,\text{Wm}^{-1}\,\text{K}^{-1}$, $\delta_\text{p} = 1.5 \times 10^{-3}\,\text{m}$, $u_\text{ci} = 0.1$ (when u_hi varies) $Re_\text{c} = 193$, $d_\text{c} = 0.002\,\text{m}$.
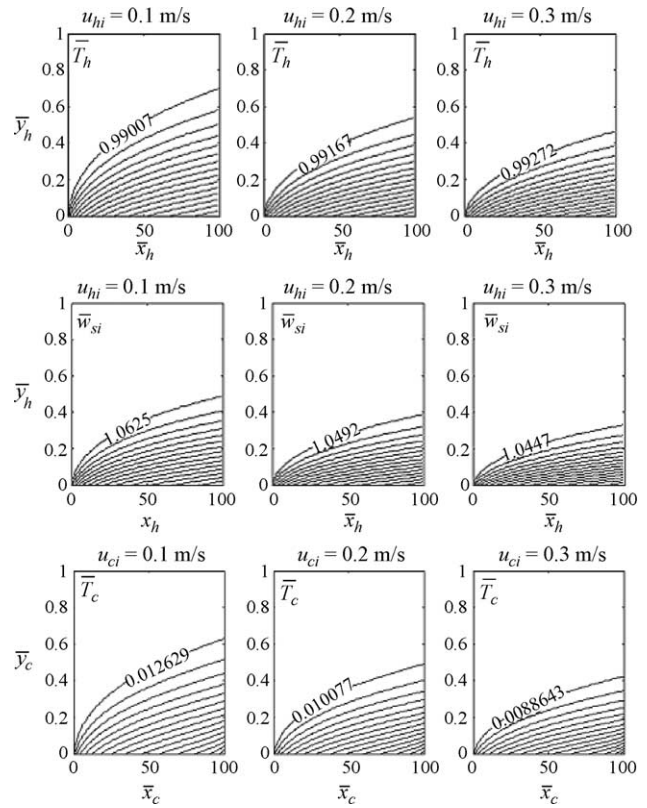

Fig. 15. Lines of constant temperature, and concentration in the hot and cold solutions for $T_\text{hi} = 70\,^\circ\text{C}$, $w_\text{si} = 0.025$, $T_\text{ci} = 20\,^\circ\text{C}$ $d_\text{h} = 0.002\,\text{m}$, $l_\text{m} = 0.2\,\text{m}$, $\delta_\text{m} = 4 \times 10^{-4}\,\text{m}$, $\chi = 1.5$, $k_\text{m} = 0.2\,\text{Wm}^{-1}\,\text{K}^{-1}$, $\varepsilon = 0.78$, $\delta_\text{g} = 2 \times 10^{-3}\,\text{m}$, $k_\text{p} = 60\,\text{Wm}^{-1}\,\text{K}^{-1}$, $\delta_\text{p} = 1.5 \times 10^{-3}\,\text{m}$, $d_\text{c} = 0.002\,\text{m}$. Re_h varies from 464 to 1393 as u_hi varies from 0.1 to 0.3 m/s and Re_c varies from 193 to 583 as u_ci varies from 0.1 to 0.3 m/s.

Fig. 16 shows that the process thermal efficiency (η_t) is hardly influenced by the inlet velocities of the hot and cold solutions, because the increase of these velocities raises J, $\tilde{Q}_\text{L}$, and $\tilde{Q}_\text{C}$ and the effects of both on η_t are slight and opposite, and the thermal efficiency is thus hardly affected. It appears from all these results that only marginal improvements can be made in the process efficiency by improving the heat transfer in the hot and cold solution channels.

5.4. The effect of the air/vapor gap width

Fig. 17 shows the permeate flux as a function of the air/vapor gap width δ_g. The permeate flux increases 2.6-fold as δ_g is reduced from 5 to 1 mm. The increase of the permeate flux can be explained by the fact that the air gap conductivity is very low relative to the other domains between the hot and cold solution, and it thus creates a high temperature, and consequently vapor pressure drop across it.

Fig. 18 shows that as the air gap width is reduced from 5 mm to 1 mm, the heat transferred by conduction, $\tilde{Q}_\text{C}$ increases 3.4-fold, and the process thermal efficiency decreases slightly, with the rate of decrease of both being more significant for δ_g smaller than 2 mm. The main purpose of the air gap
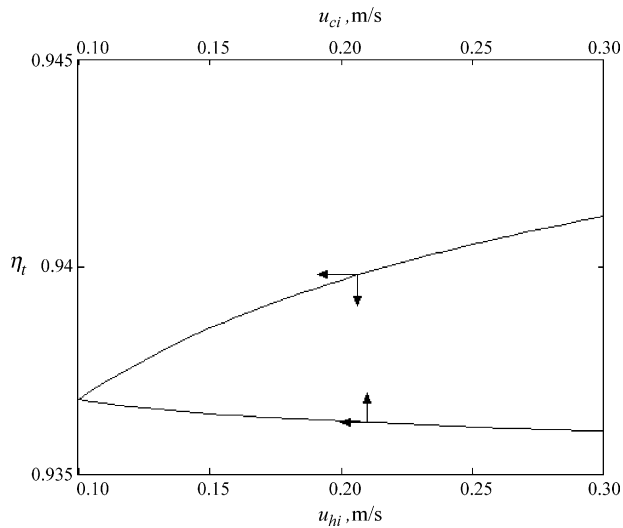
Fig. 16. Process thermal efficiency (η_t) as a function of the hot (u_{hi}) and cold (u_{ci}) solution inlet velocities. $T_{hi} = 70\,°C$, $T_{ci} = 20\,°C$, $w_{si} = 0.025$, $u_{hi} = 0.1$ (when u_{ci} varies), $Re_h = 464$, $d_h = 0.002$ m, $l_m = 0.2$ m, $\delta_m = 4 \times 10^{-4}$ m, $k_m = 0.2\,\mathrm{W\,m^{-1}\,K^{-1}}$, $\chi = 1.5$, $\varepsilon = 0.78$, $\delta_g = 2$ mm, $k_p = 60\,\mathrm{W\,m^{-1}\,K^{-1}}$, $\delta_p = 1.5 \times 10^{-3}$ m, $u_{ci} = 0.1$ (when u_{hi} varies), $Re_c = 193$, $d_c = 0.002$ m.

is to reduce the heat loss represented by the parasitic conduction heat flux from the membrane to the condensing surface. It can be seen from Fig. 18 that increasing the air gap produces, however, only a slight improvement of the process thermal efficiency, and none for air gap widths greater than 2 mm, because the permeate flux is reduced at the same time as seen in Fig. 17. Furthermore, the thermal efficiency is already rather high, 93% for $\delta_g = 1$ mm, and thus much improvement can't be attained. Narrower air gaps are thus preferred because they make the system more compact, and hence less expensive.
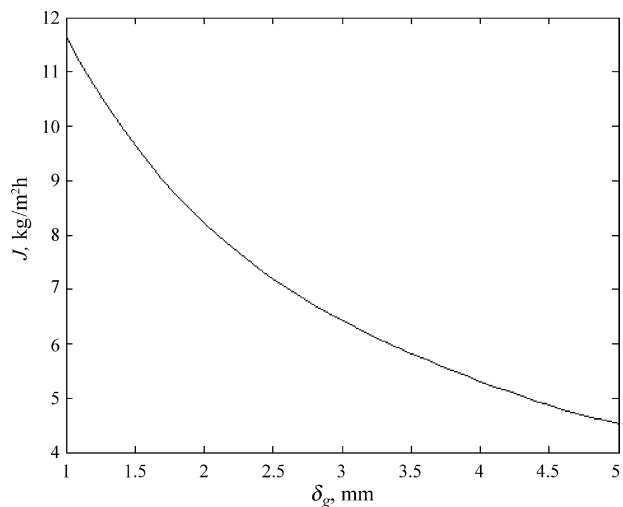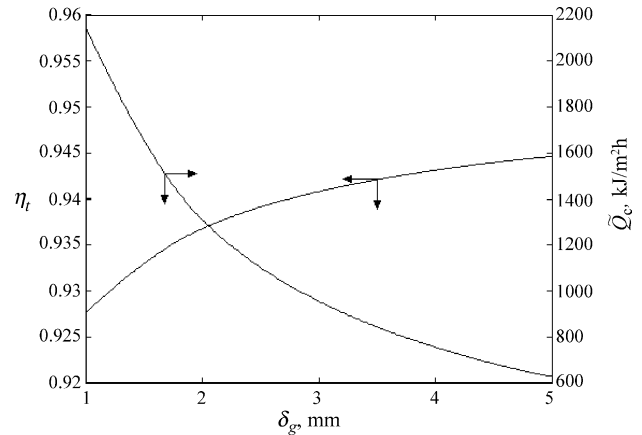

Fig. 18. The effect of the air gap width (δ_g) on sensible heat flux ($\tilde{Q}_C$) and process thermal efficiency (η_t). $T_{hi} = 70\,°C$, $T_{ci} = 20\,°C$, $w_{si} = 0.025$, $u_{hi} = 0.1$ ($Re_h = 464$), $d_h = 0.002$ m, $l_m = 0.2$ m, $\delta_m = 4 \times 10^{-4}$ m, $\chi = 1.5$, $k_m = 0.2\,\mathrm{W\,m^{-1}\,K^{-1}}$, $\varepsilon = 0.78$, $k_p = 60\,\mathrm{W\,m^{-1}\,K^{-1}}$, $\delta_p = 1.5 \times 10^{-3}$ m, $u_{ci} = 0.1$ ($Re_c = 193$), $d_c = 0.002$.

5.5. Effect of the thermal conductivity of the membrane material

Fig. 19 shows the effect of the membrane material (the solid part) thermal conductivity (k_m) on the permeate flux (J) for membrane porosities of $\varepsilon = 0.74$ and $\varepsilon = 0.84$. For $\varepsilon = 0.74$, increasing k_m from 0.05 to 0.3 $\mathrm{W\,m^{-1}\,K^{-1}}$ decreases J twofold. This decrease of the permeate flux results from the increase of the effective thermal conductivity of the membrane (k_{em}). The increase of the thermal conductivity decreases the thermal resistance and that increases the conduction heat transfer flux, which thus leaves less heat for vapor production.

For the same increase in k_m but for $\varepsilon = 0.84$, J decreases less, 1.63-fold. This is to be expected, since the increase in

Fig. 17. The effect of the air gap width (δ_g) on the permeate flux (J). $T_{hi} = 70\,°C$, $T_{ci} = 20\,°C$, $w_{si} = 0.025$, $u_{hi} = 0.1$ ($Re_h = 464$), $d_h = 0.002$ m, $l_m = 0.2$ m, $\delta_m = 4 \times 10^{-4}$ m, $\chi = 1.5$, $k_m = 0.2\,\mathrm{W\,m^{-1}\,K^{-1}}$, $\varepsilon = 0.78$, $k_p = 60\,\mathrm{W\,m^{-1}\,K^{-1}}$, $\delta_p = 1.5 \times 10^{-3}$ m, $u_{ci} = 0.1$ ($Re_c = 193$), $d_c = 0.002$ m.
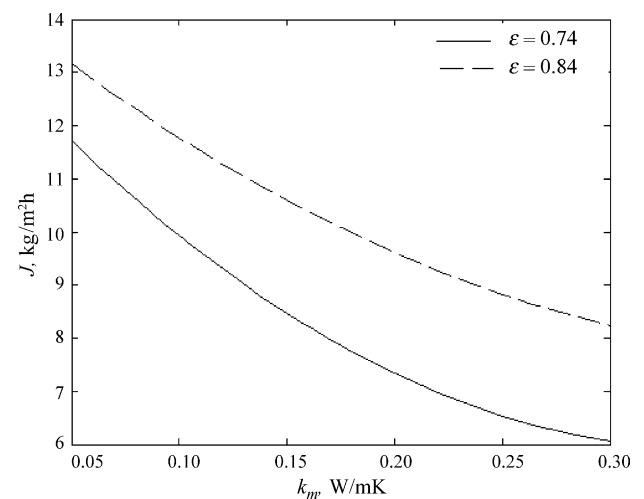
Fig. 19. The effect of the thermal conductivity of the membrane (k_m) on the permeate flux (J), for two values of membrane porosity (ε). $T_{hi} = 70\,°C$, $T_{ci} = 20\,°C$, $w_{si} = 0.025$, $u_{hi} = 0.1$ ($Re_h = 464$), $d_h = 0.002$ m, $l_m = 0.2$ m, $\delta_m = 4 \times 10^{-4}$ m, $\chi = 1.5$, $k_p = 60\,\mathrm{W\,m^{-1}\,K^{-1}}$, $\delta_p = 1.5 \times 10^{-3}$ m, $u_{ci} = 0.1$ ($Re_c = 193$), $d_c = 0.002$ m.
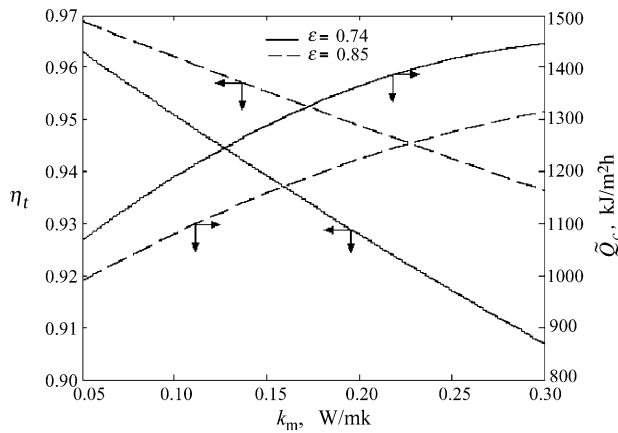
Fig. 20. The effect of the thermal conductivity of the membrane on the process thermal efficiency (η_t) and the conductive heat transfer ($\tilde{Q}_C$). $T_{\text{hi}} = 70\,^\circ\text{C}$, $T_{\text{ci}} = 20\,^\circ\text{C}$, $w_{\text{si}} = 0.025$, $u_{\text{hi}} = 0.1$ ($Re_{\text{h}} = 464$), $d_{\text{h}} = 0.002\,\text{m}$, $l_{\text{m}} = 0.2\,\text{m}$, $\delta_{\text{m}} = 4(10)^{-4}\,\text{m}$, $\chi = 1.5$, $k_{\text{p}} = 60\,\text{W}\,\text{m}^{-1}\,\text{K}^{-1}$, $\delta_{\text{p}} = 1.5 \times 10^{-3}\,\text{m}$, $u_{\text{ci}} = 0.1$ ($Re_{\text{c}} = 193$), $d_{\text{c}} = 0.002\,\text{m}$.

porosity reduces the effect of the membrane material thermal conductivity on the membrane effective thermal conductivity, k_{em}.

Fig. 20 shows that, for $\varepsilon = 0.74$, increasing k_m from 0.05 to 0.3 $\text{W}\,\text{m}^{-1}\,\text{K}^{-1}$ increases the conductive heat transfer rate by 35%. For the same increase in k_m but for $\varepsilon = 0.84$, the increase of $\tilde{Q}_C$ is 33%, and η_t decreases by about 9 and 5% for $\varepsilon = 0.74$ and $\varepsilon = 0.84$, respectively. The membrane material should thus be made of materials with small thermal conductivity for higher product flux and process efficiency. Most of the membrane materials that were used for MD experiments so far are polymers with k_{m} in the range of 0.15–0.45 $\text{W}\,\text{m}^{-1}\,\text{K}^{-1}$, although porous glass was used too, with $k_{\text{m}} = 0.78\,\text{W}\,\text{m}^{-1}\,\text{K}^{-1}$.

6. Conclusions

An AGMD process has been modeled as a two-dimensional conjugate problem in which a simultaneous numerical solution of the momentum, energy and diffusion equations of the feed and cold solutions have been carried out. The results were validated in comparison with available experimental results. The modeling and sensitivity analysis provide useful basic detailed information about the nature of the process, and are helpful for process improvement and optimization. Some of the principal conclusions are:

○ The air/vapor gap dominates the heat transfer resistance and its role in reducing the parasitic heat loss in the process is thus confirmed, the condensate film has nearly negligible relative contribution to the total resistance, and the cooling plate has nearly none.
○ Increasing the inlet temperature of the hot solution has a major effect on the permeate flux: an increase from 40 to 80 C would increase the flux by nearly an order of magni-

tude, and the thermal efficiency by 12%, while decreasing the coolant temperature has a lesser effect on the flux increase, and even slightly reduces the efficiency.
○ The feedwater salt concentration has a very small effect on the permeate flux and thermal efficiency.
○ The inlet velocities of the hot and cold solutions have a relatively small effect: tripling the saline solution velocity increases the permeate flux by 11% and the thermal efficiency is nearly unaffected.
○ The air/vapor gap width has an important effect: decreasing it five-fold increases the permeate flux 2.6-fold, but the heat transfer efficiency improves only slightly because the conductive heat loss increases too. It appears that air gap widths exceeding 2 mm do not raise process efficiency.
○ Reducing the thermal conductivity of the membrane material improves the process thermal efficiency somewhat, and the permeate flux more strongly.
○ The use of Raoult's law to model the saline solution vapor pressure predicts permeate fluxes lower by at most 4% than those predicted by empirical correlations if the feedwater solution concentration is < 10,000 ppm.

Acknowledgment

Nomenclature

A_1, A_2, A_3	see Eq. (9)
A_{h}	aspect ratio, $l_{\text{m}}/d_{\text{h}}$
c_{s}	mole fraction of NaCl
C_{p}	specific heat (kJ/kg K)
D_{s}	diffusion coefficient of the NaCl (m²/s)
d_{h}	half-width of the flow channel (m)
h_{fg}	latent heat of evaporation (J/kg)
g	acceleration of gravity (m/s²)
J	length-averaged permeate flux at the hot side of the membrane (kg/m²/h)
J_{v}	local permeate flux at the hot side of membrane, in vapor phase (kg/m²/s)
K	permeability of the membrane
k	thermal conductivity (W/m K)
l_{m}	membrane length (m)
M	molar mass (kg/kmol)
m	membrane
$\dot{m}$	mass flow rate (kg/s)
P	pressure (Pa)
Q	heat transferred (kJ/m²/h)
$\tilde{Q}$	average heat transfer (kJ/m²/h)

Q_s	sensible heat transfer (kJ/m^2/h)
R	thermal resistance (W/m^2/k)
Ra	Rayleigh number, Eq. (20)
Re_h	Reynolds number of the hot solution channel, Eq. (7).
Re_c	Reynolds number of the cold solution channel, Eq. (45)
R_{mT}	total thermal resistance of the membrane
R_s	sensible thermal resistence,
R_u	universal gas constant (J/kmol/K)
T	temperature (°C)
$\bar{T}$	$(T - T_{ci})/(T_{hi} - T_{ci})$
$\bar{T}_c$	$(T_c - T_{ci})/(T_{hi} - T_{ci})$
$\bar{T}_h$	$(T_h - T_{ci})/(T_{hi} - T_{ci})$
u_c	the velocity in x_c diection (m/s)
$\bar{u}_c$	u_c/u_{ci}
u_{ci}	the velocity at the inlet of the cold channel (m/s)
u_h	the velocity in x_h diection (m/s)
$\bar{u}_h$	u_h/u_{hi}
u_{hi}	the velocity at the inlet of the hot channel (m/s)
v	y component of feed solution velocity (m/s)
v_c	the velocity in y_c direction (m/s)
v_h	the velocity in y_h direction (m/s)
x_c	coordinate along the solution flow in the cold channel (m)
$\bar{x}_c$	x_c/d_h
x_h	coordinate along the solution flow in the hot channel (m)
$\bar{x}_h$	x_h/d_h
y_c	coordinate normal to the solution flow in the cold channel (m)
$\bar{y}_c$	y_c/d_h
y_h	coordinate normal to the solution flow in the hot channel (m)
$\bar{y}_h$	y_h/d_h
w_s	mass fraction of NaCl
$\bar{w}_s$	w_s/w_{si}
w_{si}	inlet value of the mass fraction of NaCl

Greek letters

ΔP	water vapor pressure difference between the membrane (Pa)
ΔT_g	temperature difference between the air gap hot and cold sides (°C)
β	volume coefficient of expansion (1/K)
χ	tortuosity
δ	thickness or width (m)
ε	porosity
η_t	process thermal efficiency
μ	dynamic viscosity (kg/m s)
ρ	density (kg/m^3)

Subscripts

a	air
atm	atmosphere
c	cold solution
cc	center line of cold channel
ci	inlet of the cold channel
ch	center line of the hot channel
co	outlet of the cold channel
pc	cooling plate/cold channel interface
e	effective
f	condensate film
fp	condensate film/cooling plate interface
g	vapor/air gap
gf	air gap/condensate film interface
h	hot channel
hi	inlet of the hot channel
hm	hot liquid/membrane interface
ho	outlet of the hot channel
L	latent
l	liquid water
m	membrane
mg	membrane/air gap interface
p	cooling plate
S	solution
T	Total
v	vapor

References

[1] K. Lawson, D. Lloyd, Review membrane distillation, J. Membr. Sci. 124 (1997) 1.
[2] K.W. Lawson, D.R. Lloyd, Membrane distillation. II. Direct contact MD, J. Membr. Sci. 120 (1996) 123.
[3] L. Martinez, F.J. Florido-Diaz, Theoretical and experimental studies on desalination using membrane distillation, Desalination 139 (2001) 373.
[4] J. Phattaranawik, R. Jiraratananon, Direct contact membrane distillation: effect of mass transfer on heat transfer, J. Membr. Sci. 188 (2001) 137.
[5] A.S. Jonsson, R. Wimmerstedt, A.C. Harrysson, Membrane distillation-A theoretical study of evaporation through microporous membranes, Desalination 56 (1985) 237.
[6] F. Banat, Membrane distillation for desalination and removal of volatile organic compounds from water, Ph.D. Dissertation, McGill University, Montreal, Canada, 1994.
[7] S. Bandini, C. Gostoli, G.C. Sarti, Separation efficiency in vacuum membrane distillation, J. Membr. Sci. 73 (1992) 217.
[8] G.C. Sarti, C. Gostoli, S. Bandini, Extraction of organic components from aqueous streams by vacuum membrane distillation, J. Memb. Sci. 80 (1993) 21.
[9] L. Basini, G. D'Angelo, M. Gobbi, G.C. Sarti, C. Gostoli, A desalination process through sweeping gas membrane distillation, Desalination 64 (1987) 245.
[10] M. Khayet, Paz Godino, J.I. Mengual, Nature of flow on sweeping gas membrane distillation, J. Membr. Sci. 170 (2000) 243.
[11] M. Khayet, P. Godino, J.I. Mengual, Theory and experiments on sweeping gas membrane distillation, J. Membr. Sci. 165 (2000) 261.

[12] C.A. Rivier, M.C. Garcia-Payo, I.W. Marison, U. von Stocker, Separation of binary mixtures by thermostatic sweeping gas membrane distillation I. Theory and simulations, J. Membr. Sci. 201 (2002) 1.

[13] M.C. Garcia-Payo, C.A. Rivier, I.W. Marison, U. von Stocker, Separation of binary mixtures by thermostatic sweeping gas membrane distillation II. Experimental results with aqueous formic acid solutions, J. Membr Sci 198 (2002) 197.

[14] W.T. Hanbury, T. Hodgkiess, Membrane distillation – an assessment. Second World Congr, Desalinat. Water Re-Use 3 (1985) 287.

[15] A.M. Alklaibi, N. Lior, Membrane-distillation desalination: status and potential, Desalination 177 (2004) 111.

[16] S. Kimura, S. Nakao, Transport phenomena in membrane distillation, J. Membr. Sci. 33 (1987) 285.

[17] R.W. Schofield, A.G. Fane, C.J.D. Fell, Heat and mass transfer in membrane distillation, J. Membr. Sci. 33 (1987) 299.

[18] G. Liu, C. Zhu, S. Cheung, C.W. Leung, Theoretical and experimental studies on air gap membrane distillation, Heat Mass Transf. 34 (1998) 329.

[19] S. Boguecha, R. Chouikh, M. Dhahbi, Numerical study of the coupled heat and mass transfer in membrane distillation, Desalination 152 (2002) 245.

[20] M.N. Chernyshov, G.W. Meindersma, A.B. de Haan, Modeling temperature and salt concentration distribution in membrane distillation feed channel, Desalination 157 (2003) 315.

[21] H. Kurokawa, K. Ebara, O. Kuroda, S. Takahashi, Vapor permeate characteristics of membrane distillation, Sep. Sci. Technol. 25 (1990) 1349.

[22] G.C. Sarti, C. Gostoli, S. Matulli, Low energy cost desalination processes using hydrophobic membranes, Desalination 56 (1985) 277.

[23] S. Bandini, C. Gostoli, G.C. Sarti, Role of heat and mass transfer in membrane distillation process, Desalination 81 (1991) 91.

[24] C.M. Guiji, Imre G. Racz, Jan Willem van Heuven, Tom Reith, Andre B. de Haan, Modeling of a transmembrane evaporation module for desalination of seawater, Desalination 126 (1999) 119.

[25] B.M. Fabuss, A. Korosi, Boiling point elevations of seawater and its concentrates, J. Chem. Eng. Data 11 (1966) 606.

[26] A.F. Mills, Basic heat and mass transfer, second ed., Prentice Hall, New Jersey, 1999.

[27] R.K. MacGregor, A.P. Emery, Free convection through vertical plane layers: moderate and high Prandtl number fluids, J. Heat Transfer 91 (1969) 391.

[28] J.P. Holman, Heat Transfer, Fifth ed., McGraw-Hill, New-York, 1981.

[29] FEMLAB v. 2.3, http://www.femlab.com/, COMSOL, Inc., 8 NE Executive Park, Suite 310, Burlington, MA 01803, USA.

[30] R.C. Reid, T.K. Sherwood, The Properties of Gases and Liquids: their Estimation and Correlation, second ed., McGraw-Hill, New York, 1966.

[31] J.C.S. Chou, J.R. Rowe, M. Allen, Enthalpies of aqueous sodium chloride solutions from 32 to 350 °F, Desalination 6 (1969) 105.

[32] J.D. Isdale, C.M. Spence, J.S. Tudhope, Physical properties of sea water solution: viscosity, Desalination 10 (1972) 319.

[33] S.F. Chen, R.C. Chan, S.M. Read, L.A. Bromley, Viscosity of seawater solutions, Desalination 13 (1973) 37.

[34] D.T. Jamieson, J.S. Tudhope, Physical properties of sea water solutions: thermal conductivity, Desalination 8 (1970) 393.